

4. SUBTASK 3 – PROPOSE SIMPLIFIED METHOD TO OBTAIN MIXTURE CREEP COMPLIANCE

Since the IDT creep and strength data represent critical inputs in the MEPDG software it becomes important to revisit the IDT strength and creep test methods and analyses to find out if similar information can be obtained from other simpler tests.

Obtaining Creep Compliance from DC(T) Test

Since the IDT creep test may not be available in many labs due to its relatively high cost and complexity, a surrogate tests that can be run in conjunction with the DC(T) is under investigation (creep results obtained prior to running fracture test). This concept is illustrated in Figure 1.

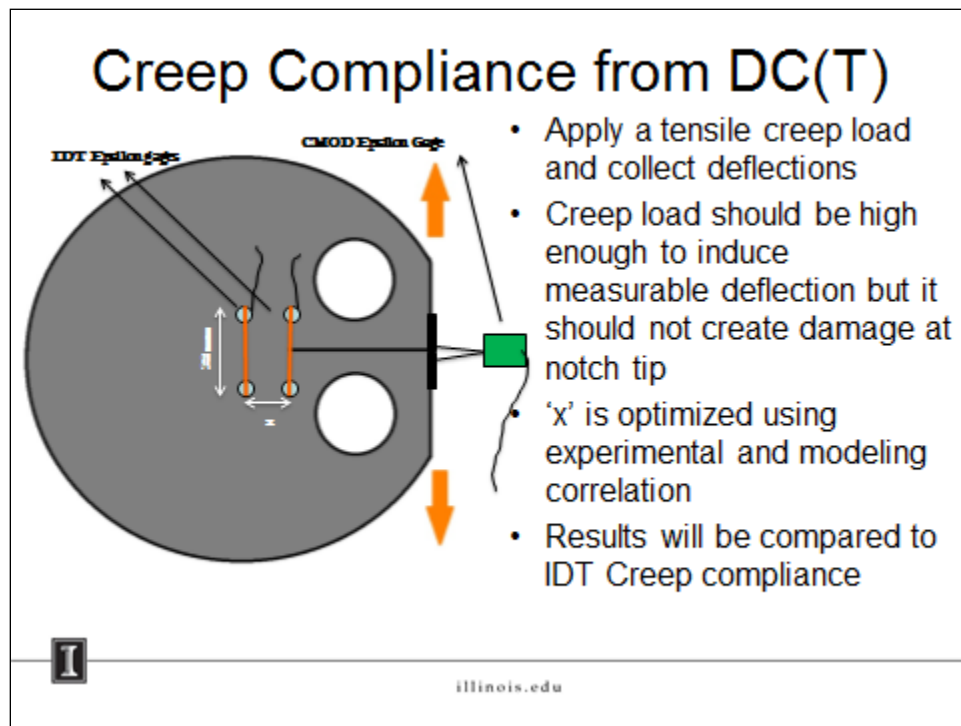


Figure 1. Concept of obtaining creep compliance from DC(T) test

A key question that needed to be answered in order to assess the feasibility of such an approach was: “can a creep test be performed on a DC(T) specimen prior to fracture testing without compromising the integrity of subsequently obtained fracture data? It was also necessary to check whether or not the creep data obtained from the DC(T) test would be comparable to the data obtained from the IDT.

The IDT creep testing procedures are specified in AASHTO T322-07. In the combined creep/fracture test, a static tension load is applied on the DCT sample and extensometers are used to measure deflections at the notch tip on both faces of the sample. The extensometers are the same ones specified for creep testing in the Superpave Indirect Tension Test (IDT), specified AASHTO T322-07, which in the case of the Advanced Transportation Research and Engineering Laboratory (ATREL), involved the use of Epsilon 3910 series extensometers. By placing the extensometers slightly ahead of the crack tip, bulk material tensile straining can be measured during a creep test, which is in turn used to obtain creep compliance from the DC(T) testing arrangement. Once the creep test is completed, the DC(T) sample is allowed to recover. After recovery, the sample is tested for fracture energy using the ASTM D7313-07 standard. Figure 2 illustrates the concept of the combined creep/fracture test. Finite element modeling is being used to obtain a conversion factor to convert measured deformation and creep load to creep compliance, as explained in a later section. Figure 3 shows typical creep data obtained from the combined DCT-IDT test.

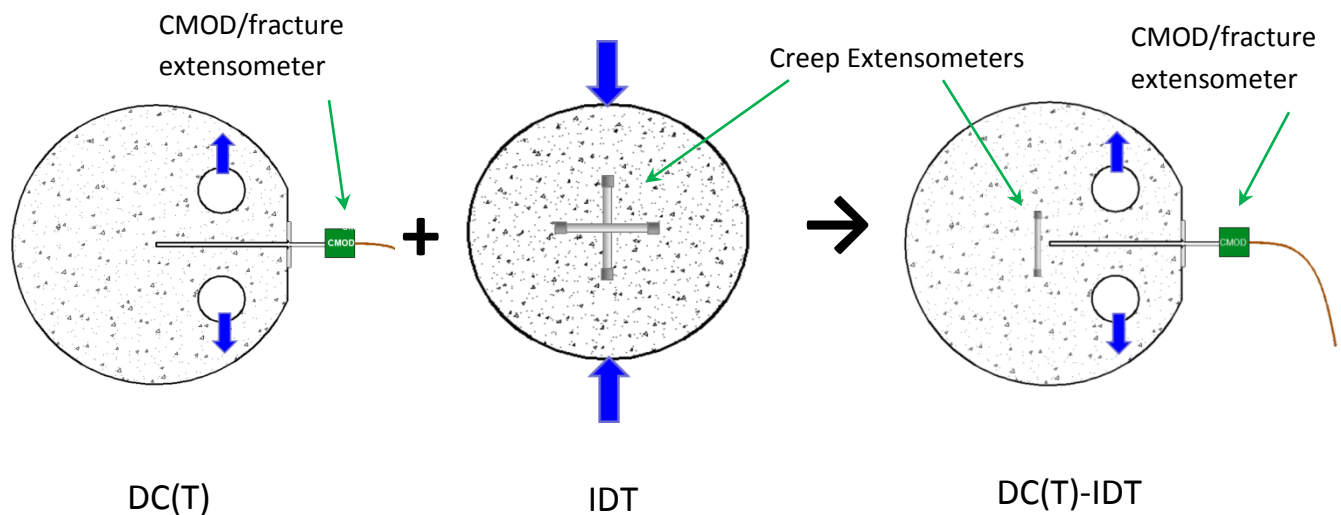


Figure 2. Comparison of Disk-shaped Compact Tension [DC(T)] test, Indirect Tension Test (IDT) and combined DC(T)-IDT test geometries.

Laboratory testing was conducted to evaluate whether or not conducting creep testing prior to fracture testing causes enough damage to significantly affect the measured fracture energy of the mix. This focused study involved testing 3 DC(T) samples for fracture energy and 3 DC(T) samples for both creep compliance and fracture energy. Preliminary tests were first conducted to determine the level of creep loading required obtaining strain responses in the extensometers that were within the allowable ranges specified in AASHTO T-322. Required creep loads were generally in the 1.5 kN range. After creep testing was completed, samples were allowed to recover for 24 hours and the fracture energy test was then conducted.

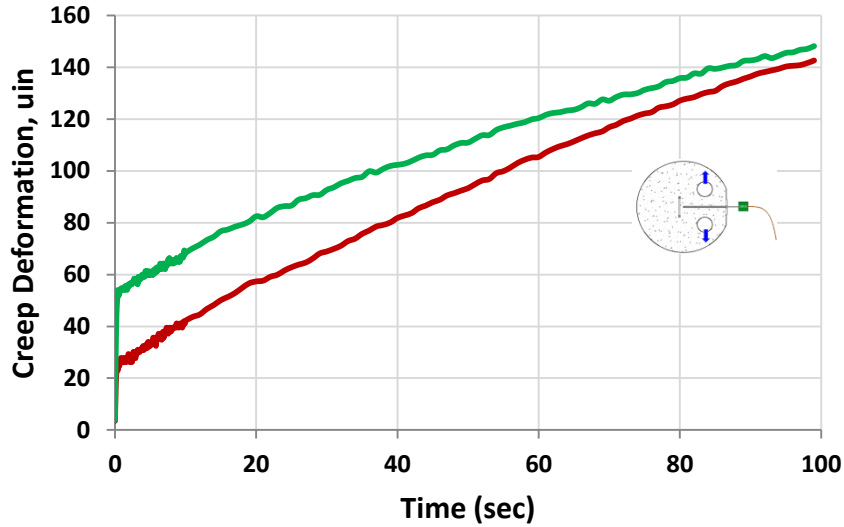


Figure 3. Typical Creep Deformation Results in DC(T) - IDT Test obtained from Surface Mounted Extensometers

The fracture energy test results suggest that there is no statistical difference between the fracture energy of the DC(T) samples tested only for fracture energy versus those tested for both creep compliance and fracture energy. Table 1 shows the comparison of the two fracture energies, with population means differing by around 1.5%. Since the typical coefficient of variance for the DC(T) test is around 9-10 percent, the difference obtained was statistically insignificant.

Table 1. Fracture Energy for Creep + Fracture versus Fracture Only Testing

Condition	Peak Load (kN)	Average Peak Load (kN)	Fracture Energy (J/m ²)		
			CMOD	CMOD average	CMOD CoV
Creep followed by fracture	3.3	3.4	346.0	371.7	9.3
	3.2		358.0		
	3.7		411.0		
Fracture testing only (control)	3.3	3.4	371.0	377.3	5.6
	3.5		360.0		
	3.3		401.0		

The above result suggests that conducting creep compliance testing followed by fracture testing on asphalt concrete samples in the DC(T) geometry may not compromise the traditional DC(T) fracture energy test results. Thus, for agencies wishing to control thermal cracking using both fracture and creep limits, such as in the case of mixtures containing significant amounts of RAP, it may be possible to conduct both tests with a single test apparatus (the DC(T) test apparatus). This could limit test device expense to under \$50k, as opposed to the need for >> \$100k of equipment, if both fracture and creep test apparatus was needed. Further work is needed to validate this result for a broader range of mixtures and to determine if a shorter rest period could be used; however, the preliminary results are very encouraging.

Finite Element Simulations

In the current study, an attempt was made to use finite element technique in conjunction with a cohesive zone model (CZM) to simulate the DCT-IDT test. Simulation of the new testing method is performed using the commercially available finite element software, ABAQUS, considering two-dimensional (2D) plane stress condition. Four-noded quadrilateral (Q4) elements were used to represent the asphalt mixture material. In addition to Q4-type elements, 2D bi-linear cohesive zone elements were embedded in the finite element model along pre-defined crack path. Various element sizes were used to develop the model. In critical region, along the horizontal diameter of DCT sample, element size reduced to 1mm×1mm. Special care was taken to keep the aspect ratio close to 1 and corner angles 90 for elements in and near the critical region. Prepared finite element model is shown in Figure 4.

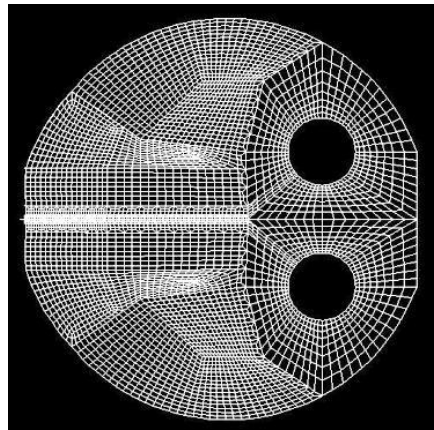


Figure 4. Finite Element Mesh of DCTIDT Sample

To investigate the effects of notch on creep deformations, two different finite element models including DCTIDT sample with and without notch were prepared. Figure 5 schematically represents samples with and without notch.

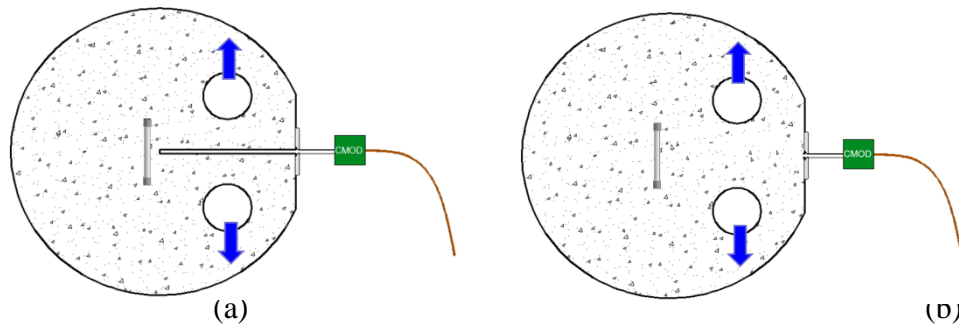


Figure 5. (a) DCTIDT sample with Notch (b) DCTIDT sample without Notch

The analyses were performed assuming modulus of 23 GPa and Poisson's ratio of 0.35 for asphalt materials. Static tensile creep load of 1kN was applied for 1000 seconds. Figures 6-8 and Figures 9-11 show the elastic simulation results of DCTIDT sample with and without notch, respectively. The objectives were:

- To determine the area where the stress distribution along the Y axis is fairly uniform and the zone is relatively unaffected by the stress concentration near the notch tip.

- To evaluate the distribution and magnitude of stresses built up inside the specimen during running creep test; making sure the induced stresses remain less than tensile strength of the material. This is done to assure there is no micro-damages that could possibly affect fracture test results, occurs during conducting creep test.

Since both models are symmetric, only the stress distribution and total deformation of half of sample (top half) are presented. The vertical stress (S_{yy}) distributions along the Y axis at different locations along the X-axis are presented in Figures 8 and 11. Comparing the stress distribution of the area located fairly close to the notch tip (2mm) and the area located just a few millimeter farther from the notch tip (10mm) shows significant drop in the stress level. The high magnitude S_{yy} observed in the immediate vicinity of the notch tip can be attributed to the stress concentration effect due to presence of notch in the sample. It is observed that the S_{yy} stress distribution becomes fairly uniform when the area is located more than 10mm away from the notch tip. The S_{yy} distribution is shown in Figure 11. Comparison of the stress distribution of samples with and without notch clearly shows the effects of notch on S_{yy} stresses. There are significant drop in stress level is observed between samples with and without notch. The total relative deformation in Y direction followed the same trend; as U_2 of samples with notch were almost three times those of sample without notch.

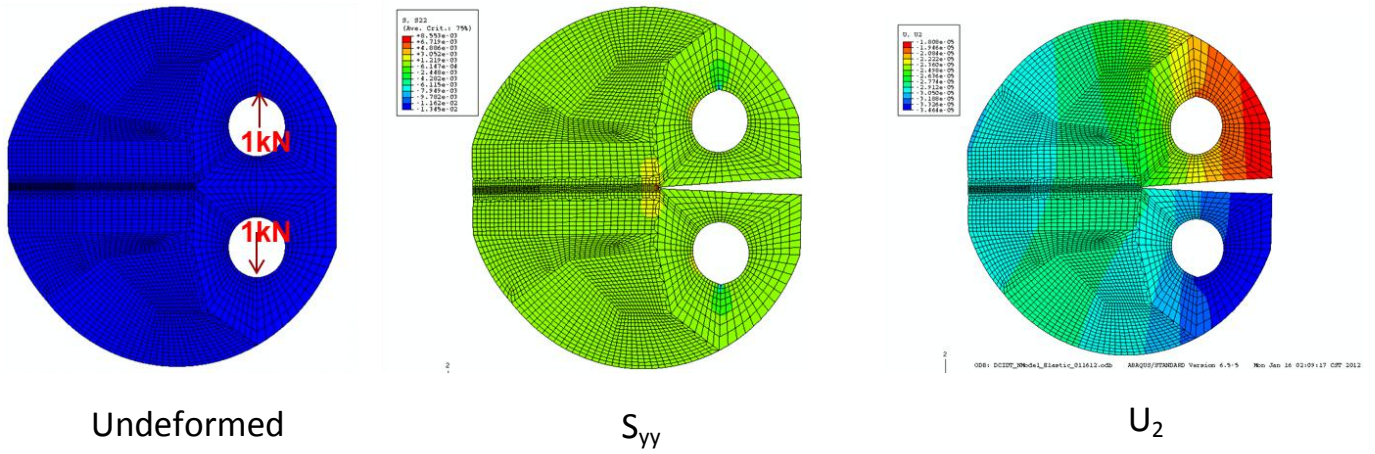


Figure 6. DCTIDT sample with Notch Elastic Model Simulation Results

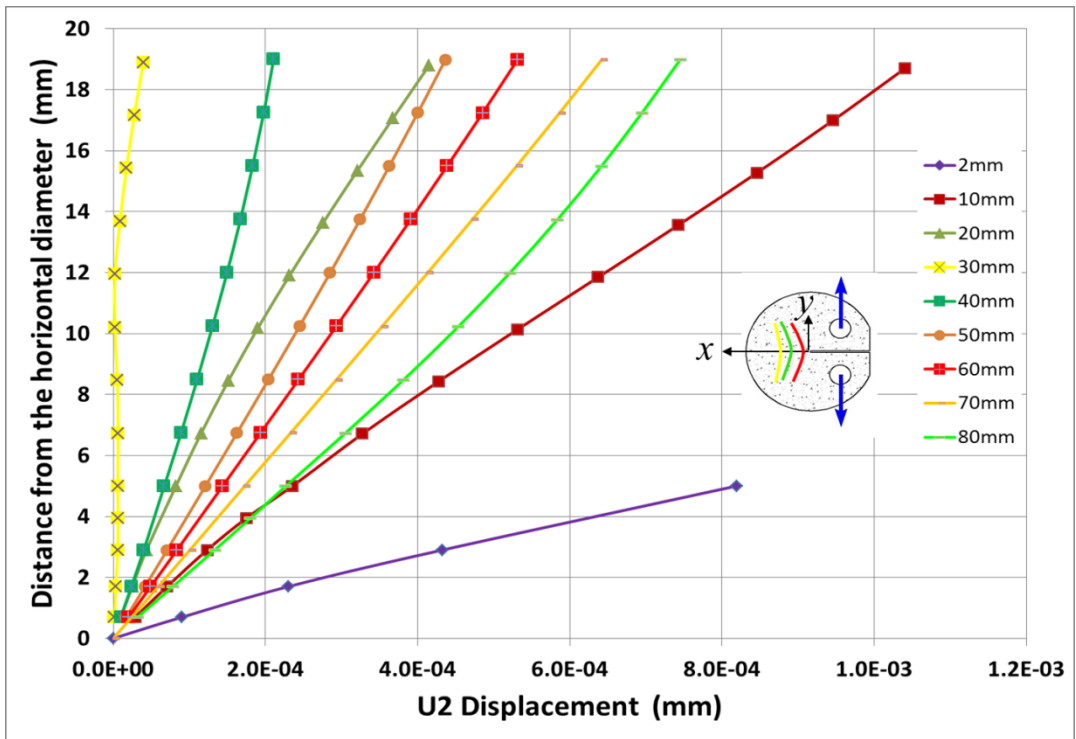


Figure 7. DCTIDT sample with Notch Elastic Simulation Results

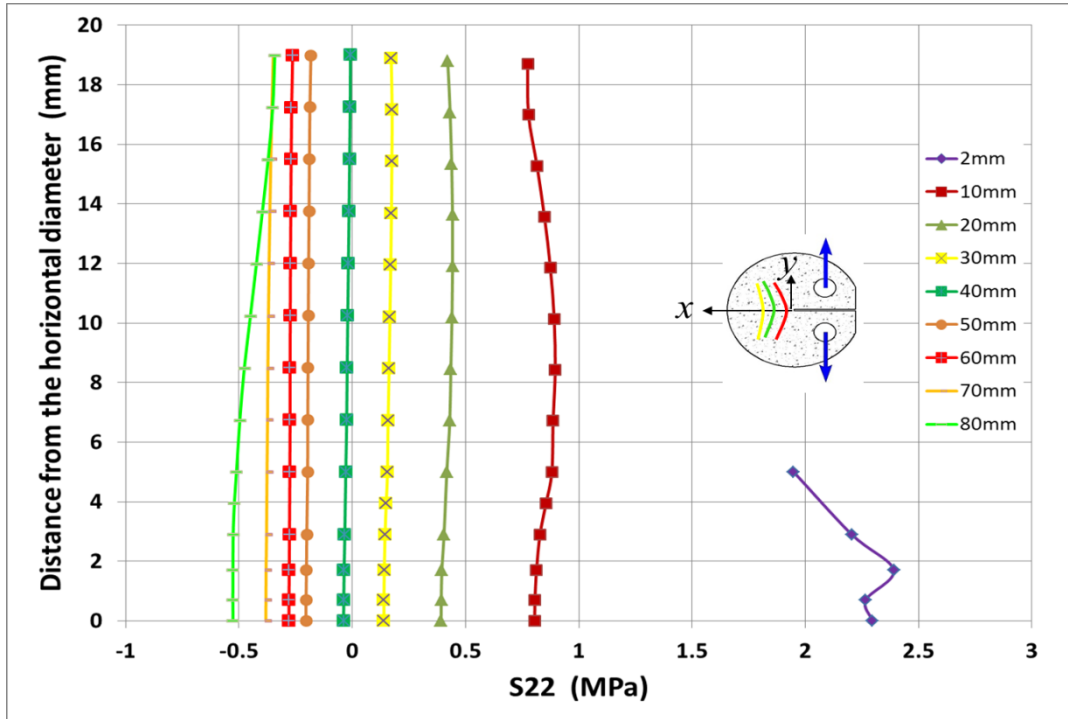


Figure 8. DCTIDT sample with Notch Elastic Simulation Results

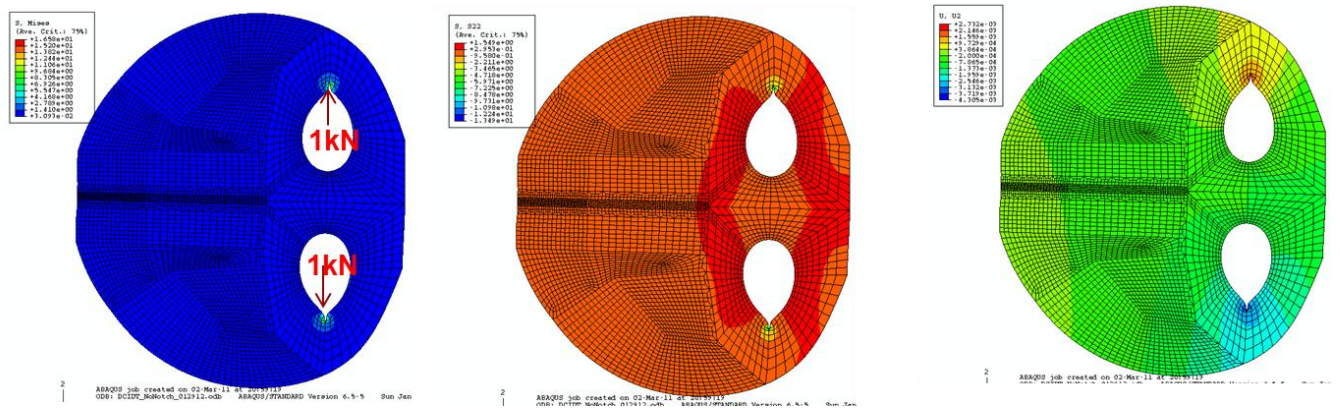


Figure 9. DCTIDT sample without Notch Elastic Model Simulation Results

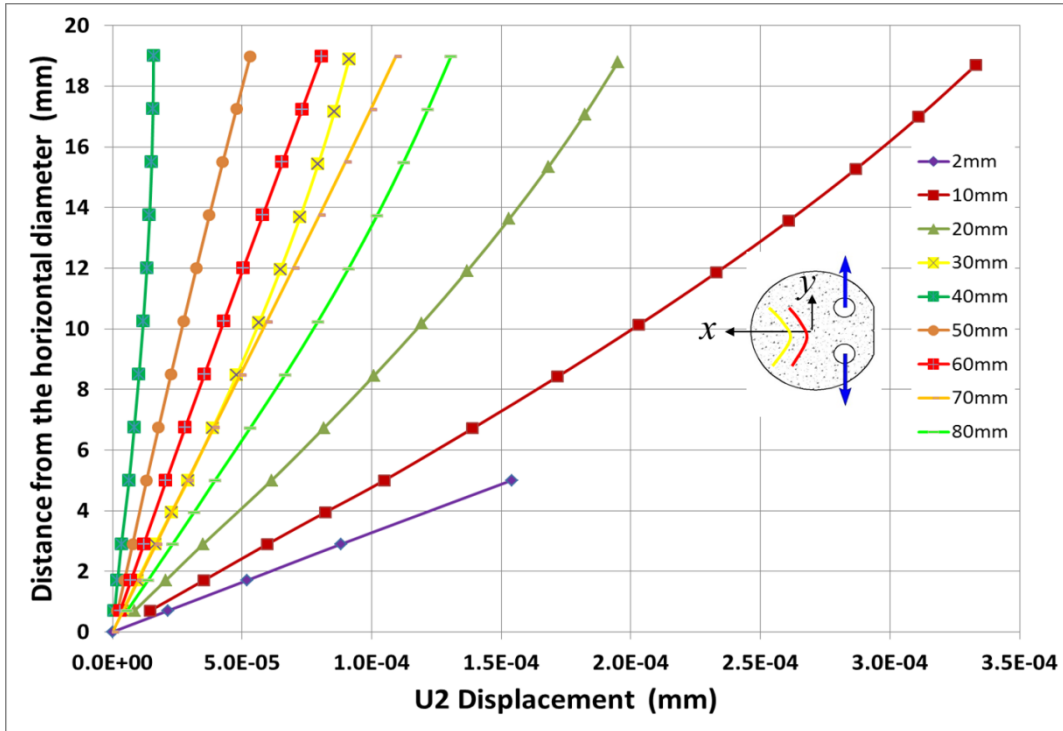


Figure 10. DCTIDT sample without Notch Elastic Simulation Results

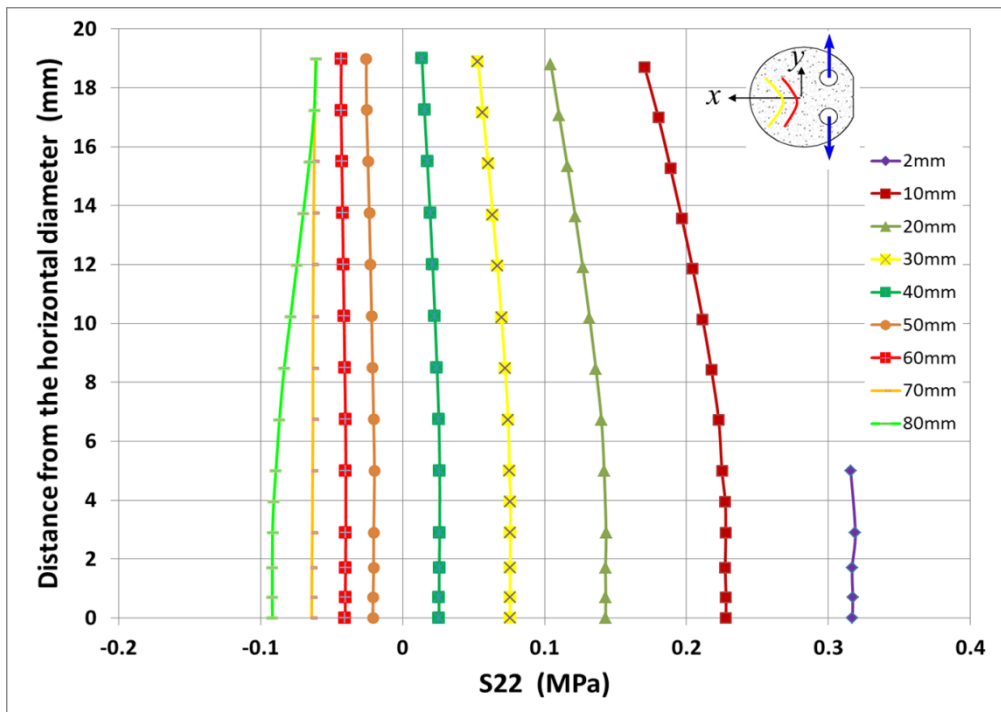


Figure 11. DCTIDT sample without Notch Elastic Simulation Results

Obtaining Creep Compliance from SCB Test

The test methodology proposed consists in using a standard notched SCB specimen to obtain both creep compliance and fracture parameters. In addition to the LLD and CMOD gauges used for fracture testing, a third gauge is employed for creep displacement measurement from a particular region of the specimen. The testing involves a mixed load and CMOD control approach. The specimen is conditioned at the desired test temperature for 2 hours and then subjected to a constant load for 1000 sec. At the completion of the creep test, the loading control is switched to a constant CMOD control to perform standard SCB fracture test. For the entire duration of creep and fracture testing, the specimen is kept in the environmental chamber. Determination of the best location for creep displacement measurement, as well as the optimal creep load, small enough to maintain the material in the linear viscoelastic region and yet produce appreciable displacements, are critical in this research investigation.

Linear Viscoelastic Conditions

Asphalt concrete is a composite material consisting of three phases: aggregate, binder and air (voids). The proportions of the components play a significant role in defining the mechanical properties of the mixture. In principle, the behavior of aggregate and asphalt binder can be idealized, as linear elastic and viscoelastic, respectively. The resulting composite material has a rather complicated behavior that is time, rate and temperature dependent (12). At low temperatures, it is fairly accurate to consider asphalt concrete as a linear viscoelastic material (13; 14), and a constitutive relationship between stresses σ and strains ε can be expressed in the form of convolution integrals by means of the Boltzman's superposition principle (15; 16):

$$\varepsilon_{ij}(t) = \int_0^t D_{ijkl}(t - \xi) \frac{\partial \sigma_{kl}(\xi)}{\partial \xi} d\xi \quad (1)$$

$$\sigma_{ij}(t) = \int_0^t E_{ijkl}(t - \xi) \frac{\partial \varepsilon_{kl}(\xi)}{\partial \xi} d\xi \quad (2)$$

$D(t)$ and $E(t)$ represent the creep compliance and relaxation modulus, respectively, and are related through a Voltera integral in equation (3):

$$t = \int_0^t E(t - \xi) D(\xi) d\xi \quad (3)$$

Several numerical methods (17; 18) are available to solve equation (3) for the relaxation modulus knowing the creep compliance since for many materials an analytical solution is not possible.

The estimation of a material parameter from stress and strain data involves an inverse problem solution. In theory, stresses and strains corresponding to sufficiently small loads and measured at a point far from the SCB specimen crack tip can be used to determine material's elastic parameters. For creep loading, the viscoelastic parameters are then easily derived through the elastic-viscoelastic correspondence principle. However, asphalt concrete is a non-homogeneous material composed of aggregate, asphalt and air, and each component has different material properties. Thus material parameters derived from point measurements may not be accurate. To overcome this problem, the stress and strain are averaged along a sufficiently long segment. It is therefore important to identify and quantify accurately the regions of high stress concentration.

By isolating the crack and boundary governed regions, the SCB elastic region is used for the determination of the elastic and viscoelastic parameters.

Analysis of stress state in SCB specimen

Due to the complex geometry, the stress state of notched SCB specimen in three-point bending was investigated through FE analyses. For this purpose the commercially available software ABAQUS was employed.

Numerical simulations were performed using the standard dimensions and loading configuration of a SCB specimen. A two dimensional plane stress model was developed using second-order quadrilateral elements. The material was assumed to be isotropic, homogeneous and linear elastic. Thus, the bulk of the model was described through the Young Modulus E and the Poisson’s ratio ν . The initial crack notch was modeled using a seam-crack, which is a crack modeling tool provided in ABAQUS. The crack tip was meshed using rings, centered at the crack tip, of collapsed quadratic quadrilateral elements. A “single node” degeneracy method was used for the elements in the first contour so that one edge of each element collapses to zero length allowing the nodes to locate at the crack tip. This type of settings allows the introduction of square root singularity for stress near the crack tip. Very fine meshes were used near singular points where high stress concentrations are expected to occur. For the rest of the specimen, relatively coarse mesh was applied.

The SCB finite element model was first used to compute the normalized stress intensity factor Y_I for varying initial notch lengths. The results were found to be in good agreement with the well-established normalized stress intensity factor equation for SCB specimen provided by Lim et al., (11), as shown in **Figure** . This implies that the stress state, especially near the crack tip, is accurately captured by the adopted SCB finite element model. Hence, it can be used to isolate the regions of SCB specimen in which the stresses change rapidly over short distances.

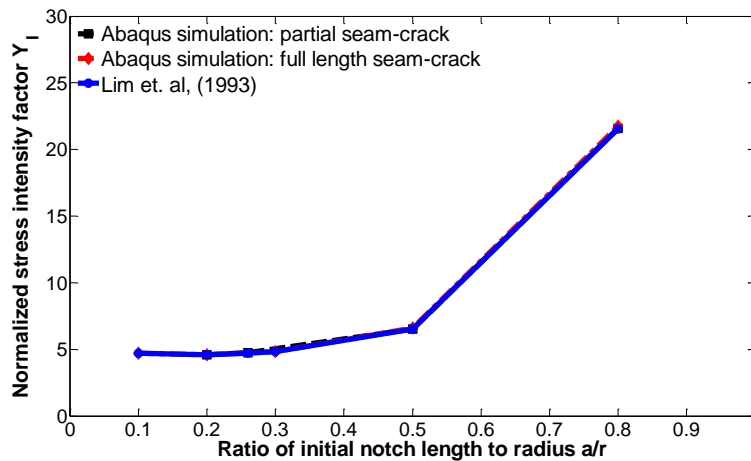


Figure 12. Verication of FE model

The stress state displayed in a SCB specimen under three-point loading is a very complex one. **Figure 11** and **Figure 12** show the Von Mises stress plots, respectively, for 1kN and 2 kN of

load. The contour scale has been adjusted in order to identify the areas in the analysis that exceeded typical strength of asphalt mixtures. The strength value was set equal to 3 MPa, very conservatively. The dark areas (colored in red in color print) represent high stress concentration, above the material strength. These areas correspond to the region near the crack tip, loading point, and vicinity of the support rollers. The sizes of these areas increase drastically with load.

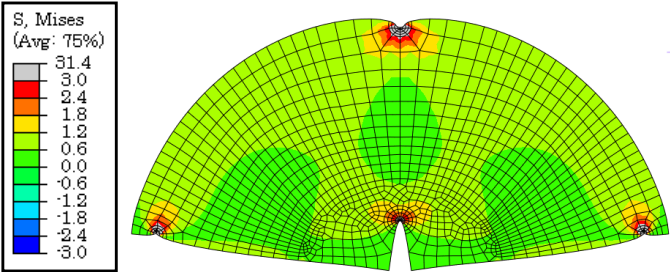


Figure 11. SCB stress state for a load of 1 kN

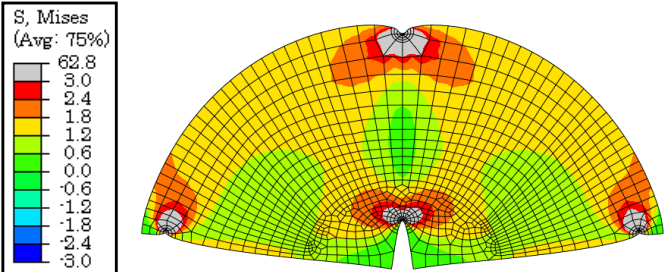


Figure 12. SCB stress state for a load of 2 kN

The plot of principal stresses, illustrated in **Figure 13**, indicates that large tensile stresses are generated at the bottom of the specimen. The principal directions, of elements in the bottom region, are parallel to the longitudinal axis-x, hence the shear stress are practically close to null. While, in the upper region a compressive arch is developed. The inclined principal stresses, in the upper region, indicate the existence of shear stress.

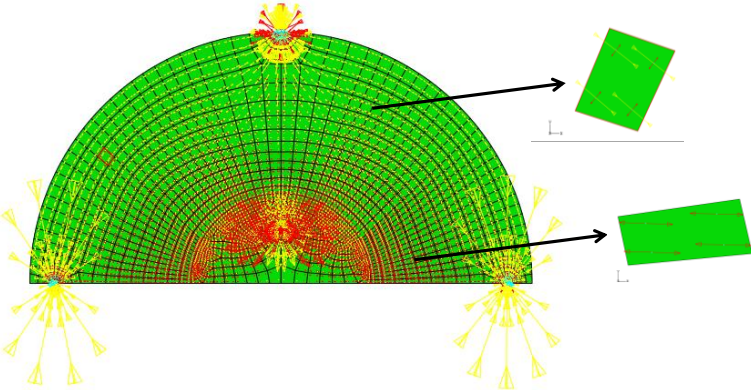


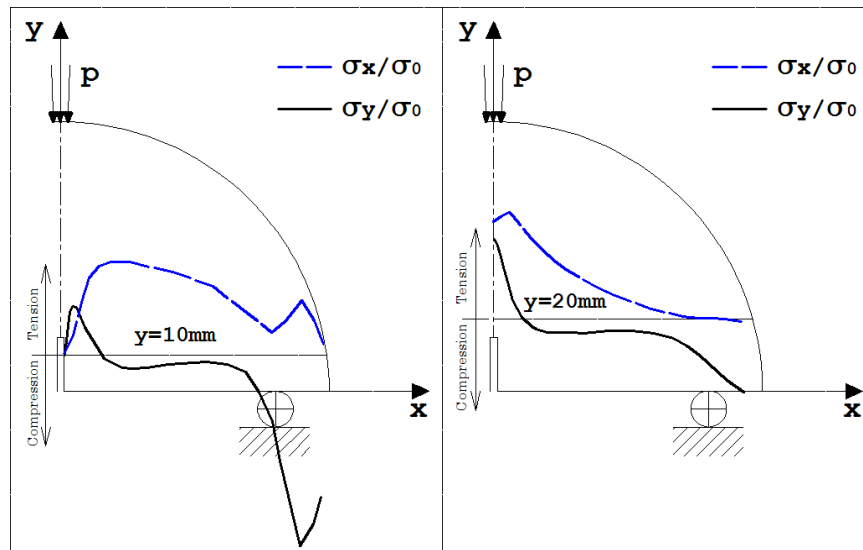
Figure 13. SCB stress state – plot of principal stress

Parametric analytical studies conducted by varying the material constants, E and ν , indicated that the stress state in a SCB specimen subjected to three-point loading is independent of the material constants. Thus, the stresses developed in an elastic SCB specimen subjected to a three-point bend test are similar to those in a viscoelastic SCB specimen tested at the same condition. This behavior is analogous to that observed in testing IDT specimens, in which the equations for the stresses along the central x and y axes are independent of material constants and remain unchanged when subjected to Laplace transforms (19). In addition, in order to apply the Laplace transforms, the stresses need to remain constant in time. The variation of stresses in time in a three point bending tests of a standard SCB specimen was analyzed through a viscoelastic FE model, and discussed in the next section.

The SCB elastic finite element model, with a notch of 15 mm, was used to analyze the stress distribution along several paths, on the SCB specimen surface, that could be used for displacement measurements. The transverse σ_{xx} and the vertical stresses σ_{yy} along the considered paths are shown in **Figure 14**. For the purpose of finding an approximated creep compliance equation, the shear stresses in the upper region of the SCB specimen were neglected. This assumption allows computing normal strains from displacement measurement obtained from a horizontal (parallel to the x -axis) trajectory. The stresses in the plot are normalized by the nominal stress σ_0 .

$$\sigma_0 = \frac{P}{bD} \quad (4)$$

where b and D represent, respectively, the thickness and diameter of the specimen.



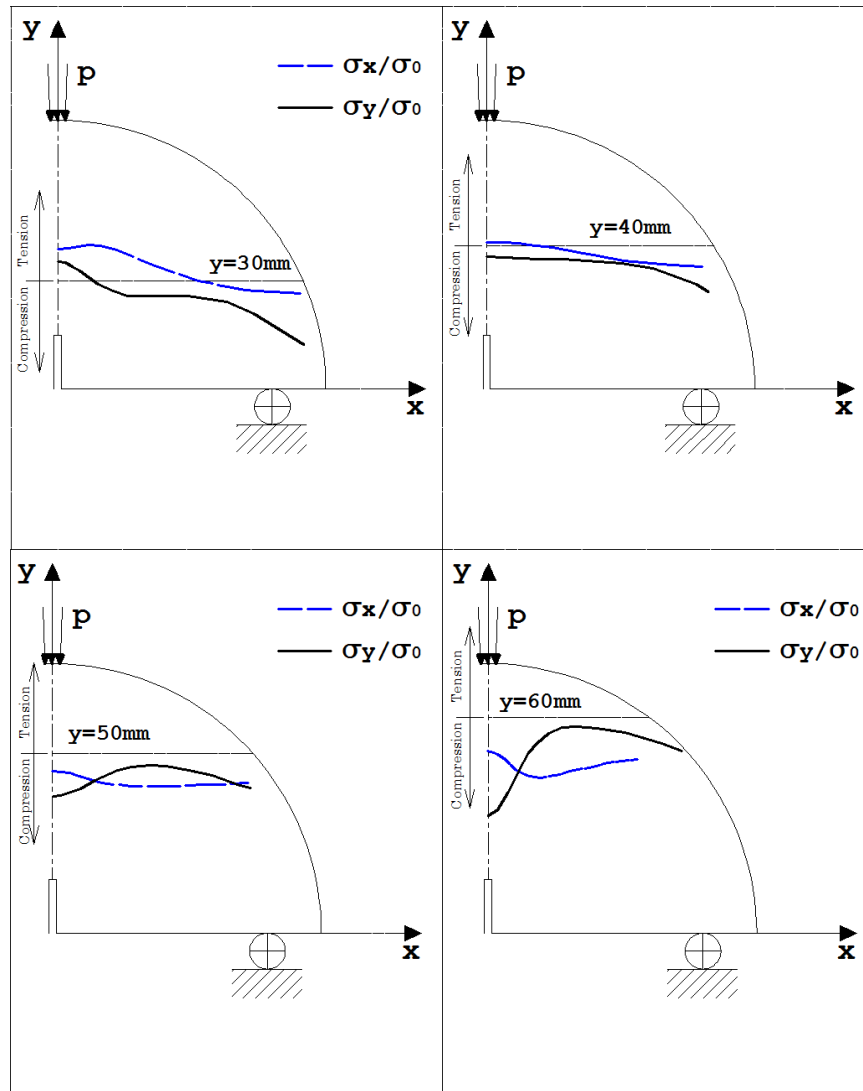


Figure 14. Stress distribution along several horizontal trajectories in SCB specimen

The trajectories that provide a sufficiently long segment in which the stresses have the same sign (tension or compression) and are almost uniform are favored. For $Y=10$ mm (10 mm from the x -axis) the stresses are almost uniform in the middle region but exhibit an abrupt change near the crack tip and the support rollers. It might be difficult to accurately identify a segment not affected by the boundary induced stresses. The stress distribution in the $Y=20$, $Y=30$, $Y=40$, and $Y=60$ trajectories exhibit one or all of the following: rapid change of slope, lack of sufficiently long segment with same sign of stresses. In contrast, a significant portion of the trajectory identified as $Y=50$ mm exhibits uniform distribution of the considered stresses. In addition, the stresses do not change drastically at both ends of this line. Based on the analyses of stress distributions, two strips (see **Figure 15**) having the central axis located, respectively, at 10 mm and 50 mm from the base of the specimen were selected for further investigation. The thickness of the strips was set to 5 mm in order to reflect the diameter of button gauge used in experiments.

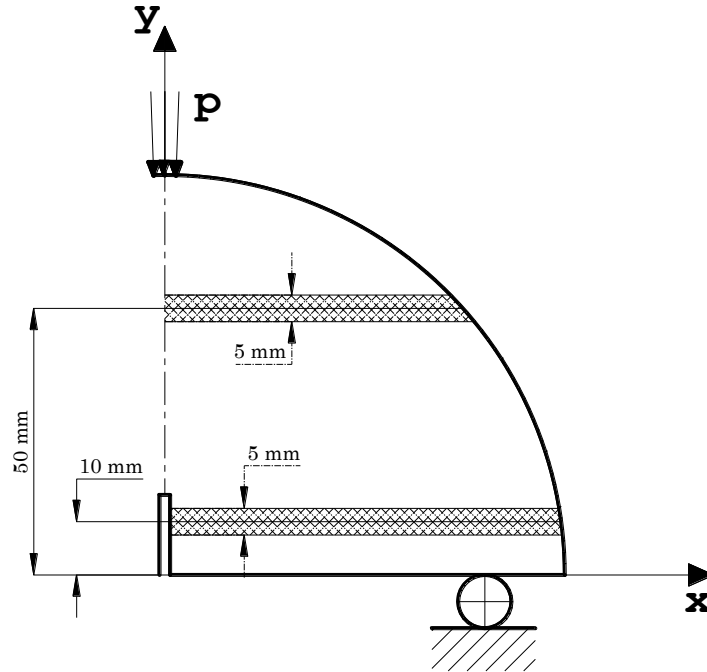


Figure 15. Potential SCB profiles for displacement measurements

The variations of the stresses along the thickness of the displacement measurement strips identified in **Figure 15** were analyzed. The stresses along the lower and upper segments of the strips were obtained from FE analysis and the percent relative differences were computed through:

$$\text{var}[\%] = 100 \frac{|\sigma_i - \sigma_j|}{\max(|\sigma_i, \sigma_j|)} \quad (5)$$

The results are plotted in **Figure 16** and **Figure 17**. The variation of transversal stresses along the thickness of the top strip is moderately significant. However, far from the central y-axis remains almost constant. While in the top strip, the variation fluctuates strongly throughout the length of the strip. The variation of the vertical stresses in the top strip is very small; the variation of vertical stresses in the bottom strip is considerably large.

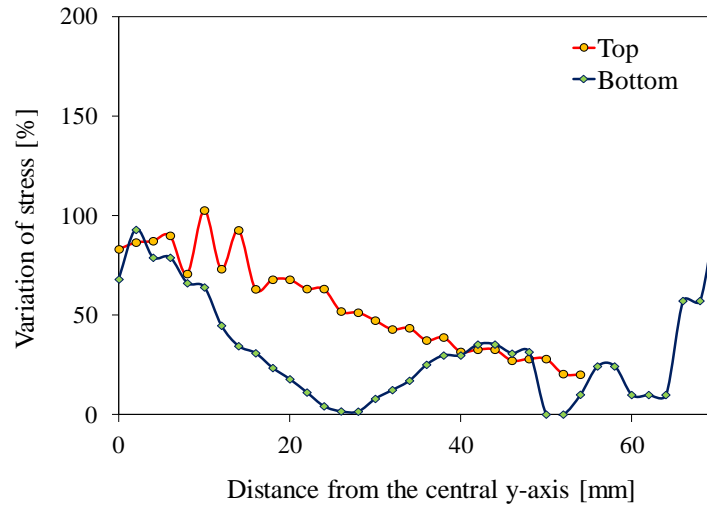


Figure 16. Variation of transversal stresses along the thickness of the measurement strip

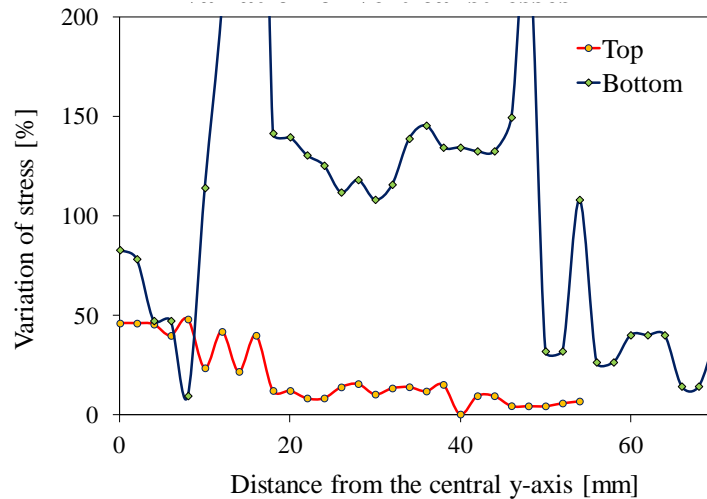


Figure 17. Variation of vertical stresses along the thickness of the measurement strip

Analysis of the effect of time on the stresses in SCB specimen

In order to investigate the variation of the stresses with time in a SCB specimen subjected to a three-point bend test, a 2D finite element viscoelastic model was developed. Asphalt concrete at low temperatures was modeled as homogeneous and linear viscoelastic material using the Generalized Maxwell Model (GMM) which is a built-in material model in ABAQUS. The viscoelastic model, presented in **Figure 8**, consisted of a single spring element representing instantaneous elasticity, and three spring-dashpot Maxwell elements to account for the relaxation that occurs in time.

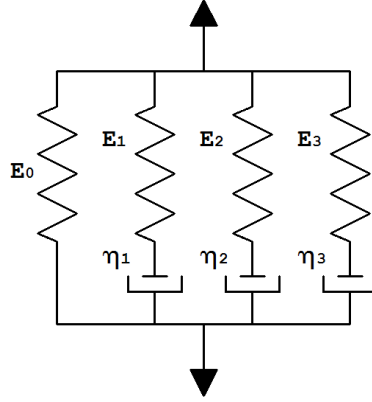


Figure 8. Generalized Maxwell Model (GMM)

The relaxation modulus for the GMM is written as:

$$E(t) = E_0 + \sum_0^n E_i e^{-\frac{t}{\rho_i}} \quad (6)$$

where E_i and ρ_i represent, respectively, the modulus and the relaxation time for the i -th spring-dashpot element. The relaxation time is the ratio of viscosity and modulus:

$$\rho_i = \frac{\eta_i}{E_i} \quad (7)$$

The GMM model parameters can be determined from experimental creep data. The creep data is fitted in 3 term Prony series model through linear and non-linear optimization methods. The resulting creep model is then converted to a relaxation function through Laplace transform. ABAQUS requests that the modulus input parameters, for the spring-dashpot elements, are given in the form of normalized shear (g_i) and bulk (k_i) modulus. The work of obtaining these GMM parameters from experimental data was performed in a previous work by Zofka (20). Accordingly, the instantaneous modulus and Poisson's ration for the model were set equal to 8.44 GPa and 0.3, respectively. The normalized shear and bulk modulus, as well as the relaxation time values are reported in **Table** .

Table 2. Input parameters for GMM model in ABAQUS

g_i [-]	k_i [-]	ρ_i [sec]
0.3542	0.3542	2.8889
0.2114	0.2114	33.0071
0.2417	0.2417	334.0924

Using the viscoelastic model, the stresses along the axis $Y=10$ mm and $Y = 50$ mm, respectively, the central axis of the bottom and the top strip, were measured at 0.5 sec and 1000 sec. The

variations computed using equation [5] are reported in **Figure 9** and **Figure 10**. It can be observed that in the middle region of both top and bottom strips, the variations are negligible. However, in the bottom strip the vertical stresses exhibit a relatively strong variation in time.

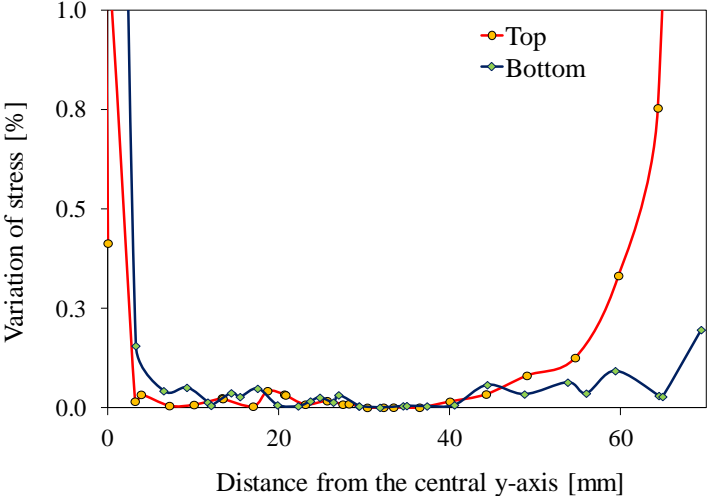


Figure 9. Variation of transversal stresses in time

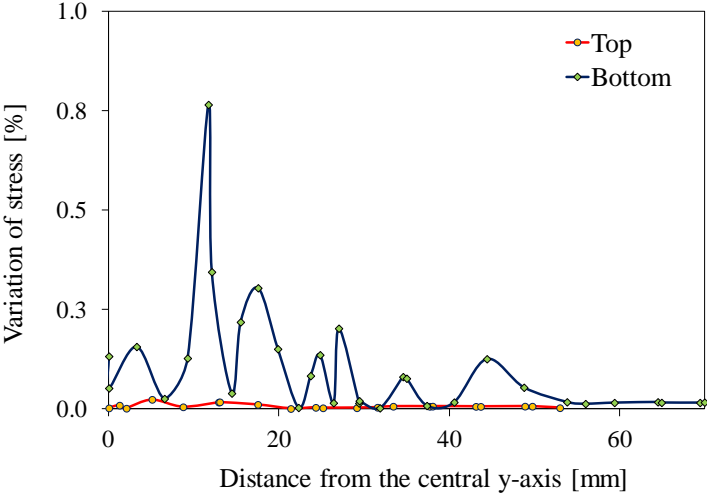


Figure 10. Variation of vertical stresses in time

Stress equations

Based on the above considerations, two segments, within the Y=10 and Y=50 axis, shown in **Figure** , were selected for experimental investigation. The length of these segments was set to reflect the length of typical strain gauge *l*. The segment located at the bottom strip displays transverse tensile and vertical compressive stresses. In the second both stresses are compressive ones. As mentioned above, the extent by which the stresses in Y=10 are influenced by the

boundary effects (crack tip and support) is difficult to accurately assess. This might cause certain degree of errors in experimental testing of materials.

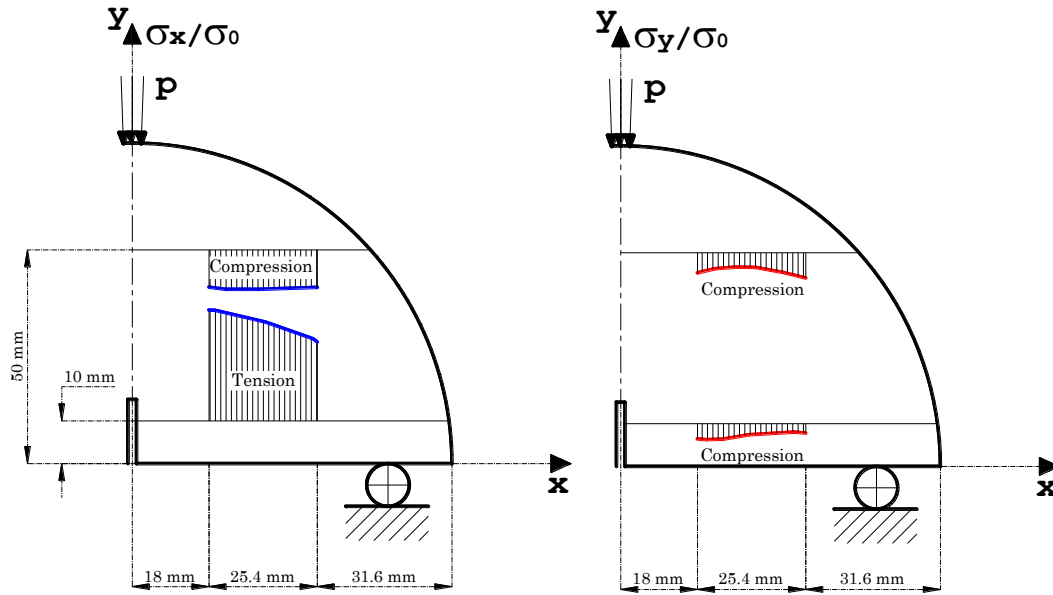


Figure 23. Segments selected for displacement measurements

The strain values for the creep function are to be obtained from displacement measurements in these segments. Whilst, the stress functions were determined numerically from the SCB finite element model and fitted into polynomial functions through the least square error (LSE) method, as shown in equation 8:

$$\sigma_x = \frac{P}{bD} (a_x x^3 + b_x x^2 + c_x x + d_x) = \frac{P}{bD} s(x) \quad (8a)$$

$$\sigma_y = \frac{P}{bD} (a_y x^3 + b_y x^2 + c_y x + d_y) = \frac{P}{bD} v(x) \quad (8b)$$

The values for the fitting coefficients are reported in **Table 3**.

Table 3. Stress function fitting coefficients

Coeff.	segment in Y= 10 mm		segment in Y= 50 mm	
	X	y	x	y
a	-0.00002	-0.00005	-0.00003	0.00004
b	0.00011	0.00189	0.00171	-0.00384
c	-0.02081	-0.00719	-0.02292	0.06122
d	2.69094	-0.37243	-1.78151	-0.98555

Equation for SCB creep compliance

An extensometer of length l is used to measure the change in length, corresponding to load P , between two points located in the selected segments. Equation 9 provides an average strain over the measurement length:

$$\varepsilon_{x,ave} = \frac{1}{l} \int_0^l \varepsilon_x dx \quad (9)$$

Equations in 8 are used to compute the average stress values through:

$$\sigma_{x,ave} = \frac{P}{bD} \int_0^l s(x) dx \quad (10a)$$

$$\sigma_{y,ave} = \frac{P}{bD} \int_0^l v(x) dx \quad (10b)$$

In a creep test loading, the load P can be described using the Heaviside step function $H(t)$ as:

$$P = P(t) = P_0 H(t) \quad (11)$$

Noting that the change in time of the average stresses is negligible (specially for stresses in the top strip), equation 11 can be substituted in equations in 10 and taking the Laplace Transform the average stress values in the s variable are obtained:

$$\hat{\sigma}_{x,ave}(s) = \frac{\sigma_{x,0}}{s} \quad (12a)$$

$$\hat{\sigma}_{y,ave}(s) = \frac{\sigma_{y,0}}{s} \quad (12b)$$

where $\sigma_{x,0}$ and $\sigma_{y,0}$ represent

$$\hat{\sigma}_{x,0} = \frac{P_0}{bD} \frac{1}{l} \int_0^l s(x) dx \quad (13a)$$

$$\hat{\sigma}_{y,0} = \frac{P_0}{bD} \frac{1}{l} \int_0^l v(x) dx \quad (13a)$$

Equation 14 introduces Hooke's law for a linear elastic material in plane stress condition:

$$\varepsilon_x = \frac{1}{E} (\sigma_x - \nu \sigma_y) = D (\sigma_x - \nu \sigma_y) \quad (14)$$

At this point, the elastic-viscoelastic correspondence principle can be used to determine the viscoelastic solution. Assuming the Poisson ratio to be time and frequency independent, the plane stress constitutive equation for viscoelastic material is given by:

$$\hat{\varepsilon}_x(s) = s \hat{D}(s) (\hat{\sigma}_x(s) - \nu \hat{\sigma}_y(s)) \quad (15)$$

Note that the stress functions were found to be independent of material constants, hence they are not altered by either Laplace or Inverse Laplace Transforms. Then the creep compliance is determined by:

$$\hat{D}(s) = \frac{1}{s} \frac{\hat{\varepsilon}_x(s)}{(\hat{\sigma}_x(s) - \nu \hat{\sigma}_y(s))} \quad (16)$$

Substituting the average stress values in equation 16 yields:

$$\hat{D}(s) = \frac{1}{s} \frac{\hat{\varepsilon}_x(s)}{(\sigma_{x,0} - \nu \sigma_{y,0})} \quad (17)$$

The Inverse Laplace Transform of equation 17 yields the creep compliance function in time:

$$D(t) = \frac{\varepsilon_x(t)}{(\sigma_{x,0} - \nu \sigma_{y,0})} \quad (18)$$

Verification of the proposed SCB creep model

The validity of the creep compliance equation proposed in this paper was checked through numerical simulation and experimental testing. The scheme outlined in **Figure 11** summarizes the verification approach adopted. Accordingly, two different techniques are used to determine the creep function of a given viscoelastic material: The proposed SCB creep test method is compared to another well-established creep test methodology. If the SCB procedure is reasonable, the different tests should yield similar creep functions.

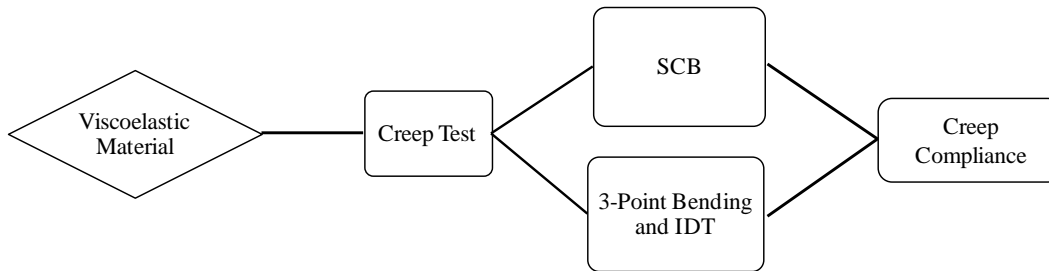


Figure 11. Validation of SCB creep model

Both numerical simulations and experimental testing were adopted. In the numerical simulation the SCB was compared to the Three-Point Bending Beam test. Whereas, in the experimental testing standard IDT test were first performed. The IDT specimens were then used to prepare notched SCB specimens on which SCB creep tests were performed. This way it was ensured that same specimens were tested by two different methods.

Numerical validation

Creep test simulations in SCB and Three-Point Bending Beam loading configurations were performed in ABAQUS. Finite element simulation

Numerical simulations of SCB and 3-Point Bending creep tests were performed in ABAQUS. The GMM model parameters in **Table** were used to define the material in both tests. Both models were modeled in 3D as simply supported structures without overhanging parts beyond the supports, see **Figure 12**.

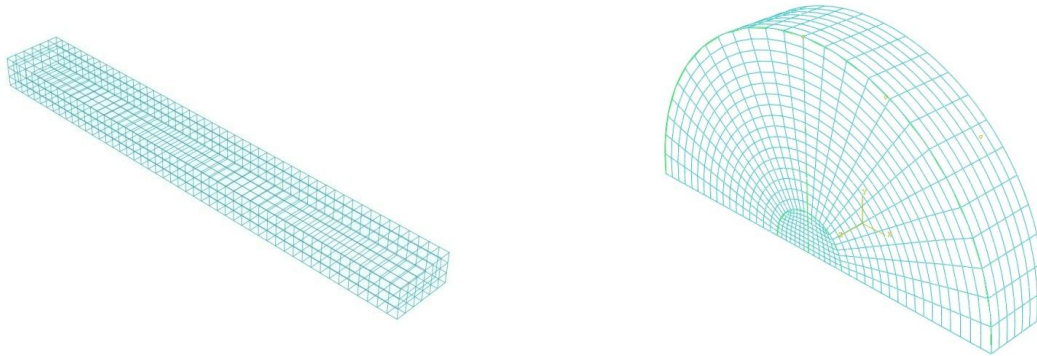


Figure 12. 3D model representations of 3-point bending and notched semi-circular beams

The dimensions of the specimens used in the numerical simulation are presented in **Table Table 4. Geometry of model beams**. The SCB model included an initial crack notch (surface) defined using a seam-crack surface with duplicate overlapping nodes in Abaqus/CAE.

Table 4. Geometry of model beams

Beam Geometry			SCB Geometry		
Height	6.35	mm	Diameter	150	mm
Thickness	12.7	mm	Thickness	25	mm
Length	101.6	mm	Notch	15	mm

Concentrated vertical compressive forces were applied in creep mode, in the middle of the beams top surface. Therefore, an instantaneous force was applied at time =0 sec and hold for 10sec.

Different meshes were tried until convergence of results was achieved. For the BBR model convergence was obtained with a mesh of 6584 brick elements C3D20R. The SCB model required 7018 wedge elements of C3D20R.

Determination of creep compliance from numerical simulations

The bending beam theory states that in the three-point bending beam, depicted in **Figure 13**, the maximum elastic deflection δ_{max} occurs at the midpoint of the span and can be computed using equation 19.

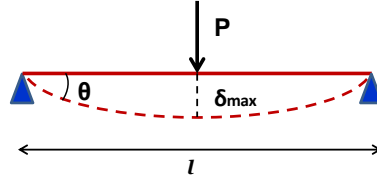


Figure 13. Schematization of 3-point bending beam

$$\delta_{\max} = \frac{Pl^3}{48EI} \quad (19)$$

where l is the length of the span, P applied load, and I moment of inertia. The equation can be modified using the elastic-viscoelastic correspondence principle and applied using creep displacement history to determine the creep compliance $D(t)$:

$$D(t) = \frac{48EI\delta(t)}{Pl^3} \quad (20)$$

Equation 19 was used to check the accuracy of the 3-point bending beam creep model. The initial elastic deflection should equal δ_{\max} . The FE model used met this requirement as it is shown in **Figure 14**.

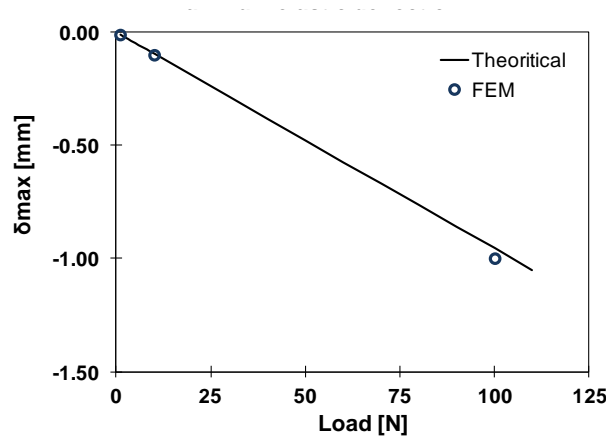


Figure 14. Calibration of the 3-point bending beam FE model

In the case of SCB creep simulation, the change in length between two model nodal points, located in the end points of the segments indicated in **Figure** , were used to determine the average strain values. Then using the stress equations proposed in equation in 8 and the creep function in equation 18, the SCB creep functions were computed.

Experimental validation

A single reference asphalt concrete mixture was used to investigate the low temperature creep function through two different test procedures: IDT and SCB. The selected mixture is part of an ongoing research project at the University Minnesota and is identified as MIF 58-34 19mm Virgin. The nominal maximum aggregate size of the mixture is 19 mm and a plain PG58-34 asphalt binder was used for its mixing.

The loose mixture was gyratory compacted into cylindrical specimens with diameter 150 mm, height 171 mm and target air void content of 7%. Three cylinders were obtained as a result of this operation. The upper and lower 10 mm layers were cut and discarded.

From each cylinder a standard notched SCB specimen was obtained for preliminary tests, from which the optimal creep load was determined. This process consisted in cyclic creep loading and unloading with increasing load to determine the load magnitude that produces appreciable displacement measurements without damaging the specimen. In addition, the peak fracture load was determined to verify that the selected creep load remains within fraction of the peak load. The optimal creep load was found to be 0.8 kN.

Three IDT specimens were obtained from each gyratory cylinder and subjected to IDT creep test according to AASHTO T 322-07 (2). A constant load of 1.6 kN, double of that required for SCB, was found to be in agreement with the standard's specification.

After IDT testing, the IDT plates were cut into SCB slice with 15mm notch. The SCB slices were then creep tested. The testing setups for both test procedure are presented in **Figure 15**.

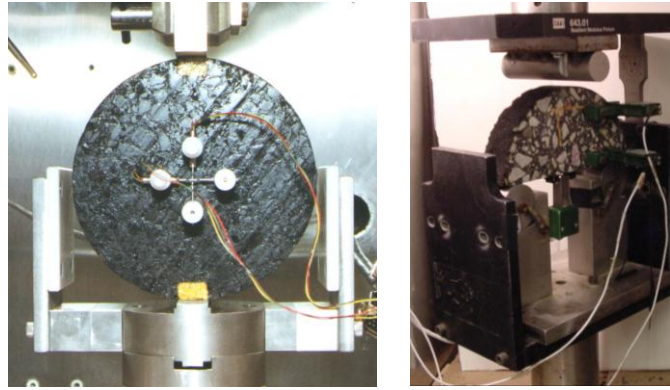


Figure 15. IDT and SCB experimental testing setup

All tests were performed in an environmental chamber at -12°C . Prior to testing the specimens were conditioned for 2 hours at the testing temperature. The load was kept for 1000 sec.

The displacement and load measured from IDT creep test are used to compute the creep compliance of the asphalt mixture according to AASHTO T 322-07. The expression for $D(t)$ is given as:

$$D(t) = \frac{\Delta X \cdot D_{avg} \cdot b_{avg}}{P_{avg} \cdot GL} \cdot C_{CMPL} \quad (21)$$

where D , b , P , and GL indicate, respectively, diameter, thickness, load, and gauge length. ΔX is the trimmed horizontal deformation and C_{CMPL} creep compliance parameter computed as:

$$C_{CMPL} = 0.6354 \cdot \left(\frac{x}{y} \right)^{-1} - 0.332$$

where x and y represent, respectively the measured horizontal and vertical deformations.

The SCB creep compliance is determined according to the procedure proposed in this section.

The creep compliance $D(t)$ functions obtained from different test set-ups, using both finite element numerical simulations and experimental laboratory tests are presented next. Additionally, the creep stiffness parameter $S(t)$ is computed as inverse of $D(t)$. The results are reported in **Figure 16** and **Figure 17**.

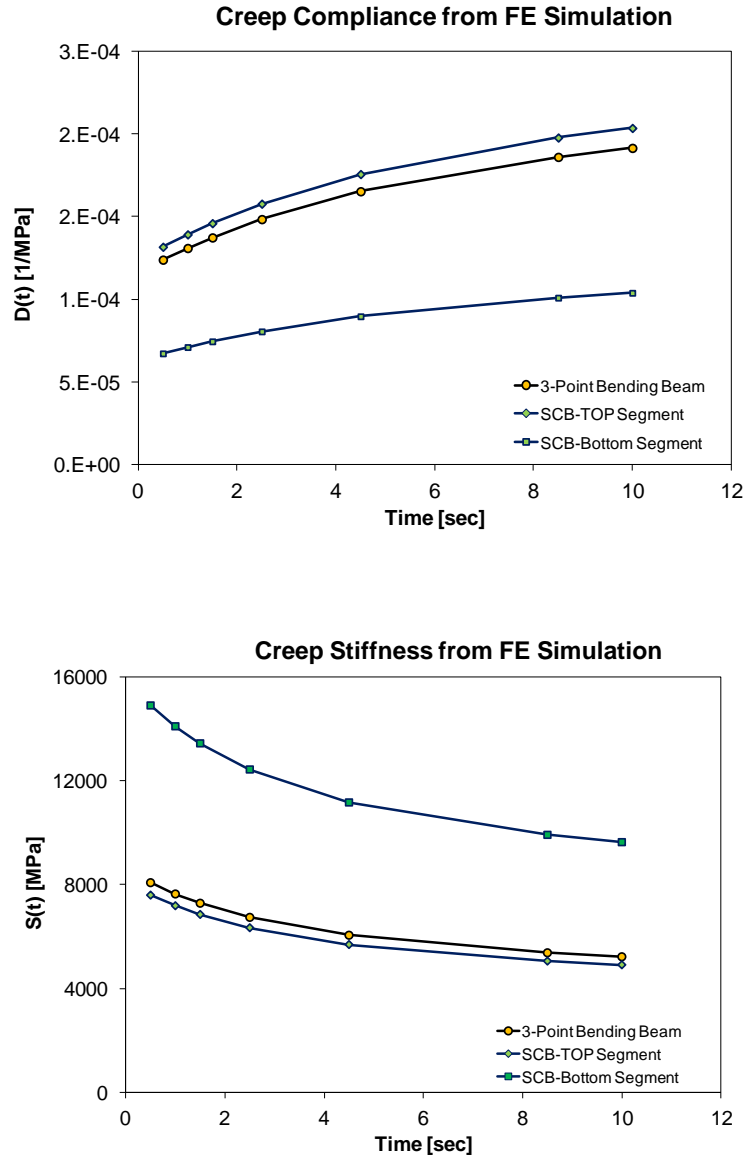


Figure 16. Results from numerical simulation

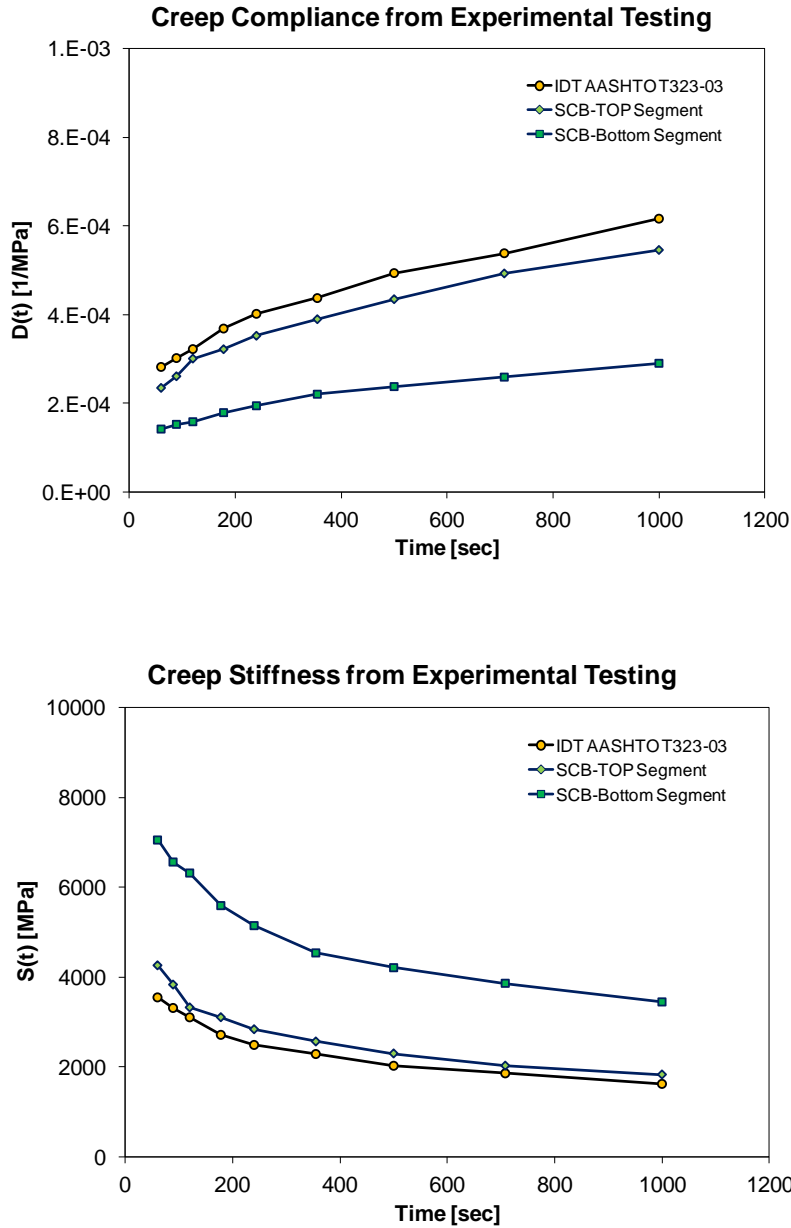


Figure 17. Results from experimental testing

The creep functions obtained from the SCB and the other two reference test configurations appear to have similar trends. However the creep compliance computed from the bottom region of the SCB is always smaller than the others. The vicinity to the crack tip and the support roller, as well as the relatively high variation of stress both in time and space observed in the bottom strip of the SCB specimen can be indicated as plausible reasons for this discrepancy. For these reasons, the average stress values used in the approximated SCB creep model described in equation 18, may not be suited for the determination of the creep function from the bottom segment. On the other hand, good agreement are obtained between the creep functions from the top segment of SCB specimen and those obtained from 3-point bending beam and IDT creep tests.

Conclusions

In this present work, the idea of determining asphalt concrete's creep compliance from the existing SCB fracture test is investigated. As a result, expressions that relate displacement measurement from particular region of the notched SCB specimen to the creep function of the asphalt concrete are derived. In particular two segments - one on the upper and another on the lower region of the SCB specimen - were identified for displacement measurement from which strains are to be computed.

The creep function computed from displacement measured at the upper segment of SCB specimen is in good agreement with creep functions from 3-point bending beam and IDT creep tests.

The findings of this research work indicate that the low temperature characterization of asphalt concrete can be entirely achieved from a single SCB test configuration. By eliminating the need for IDT creep testing, significant saving in material, time, and cost are achieved.